Biochimie 140 (2017) 34–47

Contents lists available at ScienceDirect

Biochimie

journal homepage: www.elsevier.com/locate/biochi

Research paper

Identification of two frataxin isoforms in *Zea mays*: Structural and functional studies

Celeste Buchensky [a], Manuel Sánchez [b], Martin Carrillo [a], Oscar Palacios [c], Mercè Capdevila [c], Jose M. Domínguez-Vera [b], Maria V. Busi [a], Sílvia Atrian [d], Maria A. Pagani [a], Diego F. Gomez-Casati [a, *]

[a] CEFOBI – CONICET, Centro de Estudios Fotosintéticos y Bioquímicos - Consejo Nacional de Investigaciones Científicas y Técnicas, Facultad de Ciencias Bioquímicas y Farmacéuticas, Universidad Nacional de Rosario, Rosario, Santa Fe, Argentina
[b] Departamento de Química Inorgánica, Facultad de Ciencias. Instituto de Biotecnología, Universidad de Granada, 18071, Granada, Spain
[c] Departament de Química, Facultat de Ciències, Universitat Autònoma de Barcelona, 08193, Cerdanyola del Vallès, Barcelona, Spain
[d] Departament de Genètica, Microbiologia i Estadística, Facultat de Biologia, Universitat de Barcelona, Av. Diagonal 643, 08028, Barcelona, Spain

ARTICLE INFO

Article history:
Received 3 April 2017
Accepted 15 June 2017
Available online 16 June 2017

Keywords:
Frataxin
Mitochondria
Fe-S clusters

ABSTRACT

Frataxin is a ubiquitous protein that plays a role in Fe-S cluster biosynthesis and iron and heme metabolism, although its molecular functions are not entirely clear. In non-photosynthetic eukaryotes, frataxin is encoded by a single gene, and the protein localizes to mitochondria. Here we report the presence of two functional frataxin isoforms in *Zea mays*, ZmFH-1 and ZmFH-2. We confirmed our previous findings regarding plant frataxins: both proteins have dual localization in mitochondria and chloroplasts. Physiological, biochemical and biophysical studies show some differences in the expression pattern, protection against oxidants and in the aggregation state of both isoforms, suggesting that the two frataxin homologs would play similar but not identical roles in plant cell metabolism. In addition, two specific features of plant frataxins were evidenced: their ability to form dimers and their tendency to undergo conformational change under oxygen exposure.

1. Introduction

Frataxin is a nuclear-encoded protein, highly conserved and widely present in mammals, yeast, bacteria and plants. In mammals, frataxin is mainly expressed in tissues with a high metabolic rate such as neurons, heart, kidney and liver [1]. In humans, the deficiency of frataxin is the cause of the neuro-cardio-degenerative hereditary disease called Friedreich's ataxia, characterized by the existence of mitochondrial iron accumulation and oxidative damage [2]. In yeasts, the deficiency of this protein also leads to iron accumulation in mitochondria, increased sensitivity to oxidative stress and a decrease in respiratory rate [3]. Thus, the broad distribution of frataxin in different organisms suggests an essential role of this protein related to iron homeostasis and free radical toxicity [4–6].

Various experiments show a principal role of frataxin in the iron-sulfur cluster (Fe-S) assembly and biosynthesis of cellular Fe proteins [7–9]. In *Saccharomyces cerevisiae*, it is involved in the maintenance of cell iron homeostasis, respiratory functions and protection against oxidative stress [3,10,11]. Moreover, the mature form of frataxin seems to have a mechanism that controls iron oxidation and availability *in vitro*, suggesting a possible role as iron chaperone or iron storage protein [12,13]. Also, it has been proposed that frataxin is also involved in heme metabolism in yeasts and plants [14–16]. Iron detoxification and ROS and REDOX control could be other functions of frataxin, relevant to the antioxidant defense that could play a critical role in metabolically demanding tissues [17–19]. More controversial is the matter of frataxin functional structure, and the relation of frataxin multimerization and Fe storage capacity [20,21]. These properties seem to diverge among frataxins of different taxa. Hence, while the yeast and *E. coli* proteins show no tendency to aggregate *in vivo*, but Fe induces *in vitro* the formation of high molecular weight multimers, human frataxin already aggregates *in vivo*, via protein-protein interactions of its N-terminal segment, in an iron-independent manner [22].

In plants, we have described that the *Arabidopsis thaliana* frataxin homolog, AtFH is expressed in all tissues. However, increased

* Corresponding author.
E-mail address: gomezcasati@cefobi-conicet.gov.ar (D.F. Gomez-Casati).

http://dx.doi.org/10.1016/j.biochi.2017.06.011
0300-9084/

levels of transcripts were found mainly in those tissues with high energetic demand such as flowers [9,23]. Frataxin expression in plants is essential since *A. thaliana* null mutants are lethal [9,24]; however, *AtFH knock down* plants show a decrease in heme- and Fe-S proteins activity, increased iron content and high NO levels, indicating a role also in NO signaling and oxidative stress [9,15,25]. AtFH also could complement yeast frataxin null mutants (*Δyfh1*) phenotype, suggesting a similar function in both organisms. Regardless, the role of frataxin remains elusive, especially in plants.

In non-photosynthetic eukaryotes, there is only one frataxin isoform and is located in mitochondria [1,6,26]. In yeasts and humans, frataxin homologs are synthesized as larger precursor molecules that, upon import into mitochondria, are subject to two proteolytic cleavages, yielding an intermediate and a mature form [27–30]. However, recently we have reported that in *Arabidopsis*, AtFH is dual targeted to mitochondria and chloroplasts [31], and its deficiency alters the normal functioning of the chloroplasts by affecting the levels of Fe, chlorophyll and Fe-S proteins, suggesting that AtFH would play a role both as a modulator of mitochondrial ISC and chloroplast SUF systems [31]. Although we identify only one frataxin gene in *A. thaliana*, other plants could have at least two isoforms [32]. However, this has not been verified experimentally to date.

In the present study, we have identified two genes that code for different frataxin isoforms in *Zea mays*: *ZmFH-1*, located on chromosome 1 and *ZmFH-2*, located on chromosome 3. Sequence analyses showed a high percentage of identity between both isoforms. Both proteins are functional, having a protective role against oxidants and are dual localized in mitochondria and chloroplasts. However, some differences in their expression patterns, structural features and aggregation properties were evidenced, suggesting that both isoforms would fulfill a similar but not identical function in *Zea mays* metabolism. This is the first report of the existence of two frataxin isoforms in any organism. In addition, we have confirmed the dual localization of plant frataxins in a monocotyledoneous species, and the specific features of plant frataxins of dimerization and conformational change were characterized.

2. Materials and methods

2.1. Plant material and yeast and bacterial strains

Arabidopsis thaliana var. Columbia Col-0 and *Zea mays* B73 plants, grown in a greenhouse at 22 °C with 16 h light/8 h darkness, were used in this study. *Agrobacterium tumefaciens* GV3101 strain was used for floral dip experiments.

Saccharomyces cerevisiae wild-type DY150 (MATa, ura3-52, leu2-3,112, trp1-1, his3-11, ade2-1, can1-100(oc)) and the isogenic Δyfh::his3 null mutant [3] (kindly provided by Dr. Jerry Kaplan, Utah State University) were used for the complementation assays.

Escherichia coli DH5α (*fhuA2 lac(del)U169 phoA glnV44 Φ80' lacZ(del)M15 gyrA96 recA1 relA1 endA1 thi-1 hsdR17*) and BL21 (DE3) (*E. coli* B F− dcm ompT hsdS(rB−mB−) gal λ (DE3) strains were used as bacterial hosts in cloning and expression experiments, respectively.

2.2. In silico identification and localization prediction, evolutionary analysis and molecular modeling of maize frataxins

The sequences of the two genes coding for frataxins, *ZmFH-1* (MaizeGBD #GRMZM2G083755, NCBI accession number NM_001152800) and *ZmFH-2* (MaizeGDB #GRMZM2G062342, NCBI accession number NM_001157260) were obtained by searching with the Basic Local Alignment Search Tool (BLAST), specifically the nucleotide BLASTN program, in the plant genomics resource Phyzome.11 (https://phytozome.jgi.doe.gov/pz/portal.html), limiting the results to *Zea mays*. *Arabidopsis thaliana* frataxin mRNA sequence (At4g03240.1) was introduced as a query.

Cellular localization predictions of maize frataxin isoforms were made with the GTP_pp, GTP_ref (https://plantcode.biologie.uni-marburg.de/predloc/index.php), ChloroP (http://www.cbs.dtu.dk/services/ChloroP/), Mitoprot (https://ihg.gsf.de/ihg/mitoprot.html), Predotar (https://urgi.versailles.inra.fr/predotar/predotar.html) [33] and TargetP (http://www.cbs.dtu.dk/services/TargetP/) [34] web programs.

A multiple sequence alignment of amino acid sequences for frataxins from different species was created with ClustalX2 [35]. The phylogenetic tree was constructed using Mega5 [36], applying the Maximum Likelihood method. Bootstrap support was estimated using 1000 replicates.

Homology modeling was performed using the @TOME2 server (http://atome1.cbs.cnrs.fr/AT2B/meta.html) [37]. The 3-D structural models obtained were evaluated with the ProSA-web structure analysis program [38,39] and Verify-3D [40]. Superposition of proteins structures was performed using the SuperPose server v 1.0 (http://wishart.biology.ualberta.ca/SuperPose/) [41].

2.3. Quantitative real-time PCR analysis (qPCR)

Three biological replicates, consisting each sample of leaves and roots pooled from three plants, were analyzed at each time point. Total RNA was isolated with TRIZOL®reagent (Invitrogen, Carlsbad, CA, USA) following the manufacturer's protocol and treated with DNase I (Thermo Fisher Scientific, Waltham, MA, USA). The cDNA was synthesized using Random hexamers (Amersham Biosciences, UK) from 1 μg of total RNA with the reverse transcriptase M-MLV and RNase Inhibitor (Promega, Fitchburg, WI, USA). Quantitative real-time PCR reactions were performed in a 20-μL final volume with 0.5 μM gene-specific primers (Table 1), 2 μL of cDNA as a template and SYBR Green I (Invitrogen) as the detection reagent. Maize *actin 1* (J01238) was used as a reference gene. The amplicon lengths were 190 bp for *ZmFH-1*, 102 bp for *ZmFH-2*, and 163 bp for *actin 1*. The reactions were performed in an MX3000P QPCR System (Stratagene) in triplicate (technical replicates). PCR conditions were: 95 °C for 2 min, followed by 45 cycles of 95 °C for 10 s, 62 °C for 15 s and 72 °C for 15 s. After final annealing (72 °C, 5 min), a melt curve analysis was made by increasing the temperature from 65 °C to 95 °C at 0.2 °C intervals to check the specificity of the assays. The SYBR® Green I fluorescent signal was determined for each cycle at the end of the extension step.

2.4. Plant transformation, protoplast isolation and fluorescence confocal microscopy

ZmFH-1 (codons 1–83) and *ZmFH-2* (codons 1–78) sequences containing the sequence coding for the transit peptides predicted with Mitoprot [42] and ChlroP [43] were cloned into pZP212 plasmid fused to the GFP sequence (green fluorescent protein) at the 3'end. The expression of both transcripts is under the control of the 35S CaMV promoter. The pZP212 plasmid constructs were transformed in *Agrobacterium tumefaciens* to transform *A. thaliana* plants by the floral dip method [44]. Transgenic lines were selected in MS agar medium with 50 μg/ml kanamycin for 15 days, transferred to soil, and grown at 22 °C in a greenhouse under long day conditions (16 h day/8 h night). Transformed plants were confirmed by PCR.

Arabidopsis mesophyll protoplasts isolation was performed as described by Sang-Dong Yoo et al. [45]. Rosette leaf strips were cut from the middle part of the leaf. Approximately 20 leaves were digested in 10 ml of enzymatic solution (20 mM MES (pH 5.7), 1.5%

Table 1
Sequences of the oligonucleotides used for qPCR analysis (named rt-ZmFH and rt-ZmActin), cloning into pZP212 plasmids (named tp-ZmFH), cloning into pYES3CT plasmids (named y-ZmFH), and cloning into pGEX 4T1 plasmids (named *Bam*HI-ZmFH and ZmFH-*Xho*I).

Forward oligonucleotide		Reverse oligonucleotide	
Name	Sequence	Name	Sequence
rt-ZmFH2F	AACTGGATCGAATCTTGTGCAACTTC	rt-ZmFH2R	CTAGTTGTGTGGCATTTCCTGTACTATTATG
rt-ZmFH1F	CTAGGTTTGATTGGGATGCAACAGC	rt-ZmFH1R	TGTACTACACTTCGACATTCAGAGCAC
rt-ZmActin1F	TACCATGTTTCCTGGGATTGCCG	rt-ZmActin1 R	CCACATCTGCTGCTGAAAAGTGC
tp-ZmFH2F	AAATCTAGAATGGCGTCGCCGTCG	tp-ZmFH2R	AAAAGGATCCGCGTCACTGAAGGC
tp-ZmFH1F	AAATCTAGAATGGCATCGCGTAAGCTT	tp-ZmFH1R	AAAAGGATCCACTGCAGATGGGCTAGA
y-COXIVF	AAAAAGCTTATGCTTTCACTACGTCAATCTA	y-COXIV-ZmFH2R	GCGCGTCACTGAAGGCGGACAGTTGGGCAGTTTTCACCACGGGTT
		y-COXIV-ZmFH1R	CAGACACATCTCCTGTAGACTGTTGGGCAGTTTTCACCACGGGTT
y-ZmFH2F	ACCCGTGGTGAAAACTGCCCAACTGTCCGCCTTCAGTGACGCGC	y-ZmFH2R	AAACTCGAGTTATGAAAGTTGTACTGGAGTA
y-ZmFH1F	ACCCGTGGTGAAAACTGCCCAACAGTCTACAGGAGATGTGTCTG	y-ZmFH1R	AAACTCGAGCTAAAGTTCTACTGGAGTACCA
*Bam*HI-ZmFH2F	ATTGGATCCGCCTTCAGTGACGC	ZmFH2-*Xho*I R	AAACTCGAGTTATGAAAGTTGTACTGGAGTA
*Bam*HI-ZmFH1F	ATTGGATCCGCCTTCAGTGACGC	ZmFH1-*Xho*I R	AAACTCGAGCTAAAGTTCTACTGGAGTACCA

(w/v) cellulase R10, 0.4% (w/v) macerozyme R10, 0.4 M mannitol, 20 mM KCl, 10 mM $CaCl_2$, 0.1% (w/v) BSA) at 22 °C for 12 h with gentle shaking at the end of the treatment. The suspension was filtered and protoplasts were collected by centrifugation at 150 x *g* for 5 min, followed by three washes with WI solution (4 mM MES pH 5.7, 0.5 M mannitol and 20 mM KCl). The protoplasts were incubated with 1 μM Mitotraker Orange fluorescence dye (Invitrogen, Carlsbad, CA, USA) for 30 min in the dark.

Fluorescent signals were analyzed using an inverted confocal microscope Nikon Model Eclipse TE-2000-E2, with a 60X objective. Excitation was performed at 488 nm and 543 nm for GFP and Mitotraker, respectively. For fluorescence emission, the spectral detector was set between 515 and 530 nm for GFP, between 585 and 640 nm for Mitotraker and at 665 nm for chlorophyll autofluorescence. Protoplasts from wild-type plants grown under the same conditions were used as controls for background chlorophyll fluorescence.

In addition, transformed *A. tumefaciens* cells were used for infiltration of *Nicotiana benthamiana* plants. Recombinant *Agrobacterium* culture was grown overnight at 28 °C. Cells were harvested by centrifugation and resuspended to reach a concentration corresponding to an optical density of 0.8 at 600 nm in a solution of 10 mM MgCl2, 10 mM MES pH 5.7, and 100 μM acetosyringone. Cultures were incubated at room temperature for 3 h and then *N. benthamiana* leaves were infiltrated. After one week, leaves were analyzed by confocal microscopy, as described above.

2.5. Yeast functional complementation assays

Saccharomyces cerevisiae wild-type cells (DY150) and an isogenic frataxin knockout strain (*Δyfh::His3*) were used for the complementation with chimerical constructs cloned in the pYES3CT vector system (Invitrogen). These constructs contain the *S. cerevisiae* cytochrome oxidase subunit IV (COXIV) transit peptide fused to the coding sequences of the mature ZmFH-1 or ZmFH-2 proteins (codons 70–199 and 74–201, respectively). The transformed cells were selected in synthetic medium without tryptophan with glucose as carbon source.

Transformed yeasts were grown in YP-raffinose 2% (w/v) and the protein expression was induced with galactose 2% (w/v). To evaluate the sensitivity of these cells to oxidative damage, aliquots of yeast culture with an $OD_{600} = 1$ were treated with H_2O_2 2 mM for 1 h with shaking. Serial dilutions of these cells were spotted in YP-galactose medium and grown at 30 °C for 3–4 days.

2.6. Cloning, expression and purification of recombinant frataxins

Both maize frataxins, ZmFH-1 and -2 were amplified without their transit peptides by conventional PCR (codons 70–199 and 74–201, respectively), using cDNA from maize leaves and the primers *Bam*HI-ZmFH1F, 2F and *Xho*I-ZmFH1R, 2R shown in Table 1. Amplification was performed with Taq DNA polymerase (Invitrogen) under the following conditions: 30 s at 94 °C (denaturation), 30 s at 55 °C (annealing) and 30 s at 72 °C (elongation). The primers used added 5′ *BamH*I and 3′ *Xho*I restriction sites to the ZmFH coding regions, for cloning into the pGEX-4T1 expression vector (GE Healthcare bio-Sciences, Uppsala, Sweden), downstream from the glutathione-S-transferase (GST) open reading frame to generate pGEX–ZmFH-1 and pGEX–ZmFH-2 plasmids. The absence of mutations was confirmed by DNA sequencing. Each expression plasmid was used to transform *E. coli* BL21 (DE3) cells.

For protein expression, *E. coli* cells were grown in LB medium with 100 mg mL^{-1} ampicillin. GST-ZmFH protein synthesis was induced with isopropyl-1-thio-β-D-galactopyranoside (IPTG) at a final concentration of 0.5 mM. After 3 h-induction at 37 °C, cells were harvested by centrifugation. For protein purification, cells were re-suspended in ice-cold PBS (1.4 M NaCl, 27 mM KCl, 101 mM Na_2HPO_4, 18 mM KH_2PO_4), disrupted by sonication and centrifuged at 10,000 x *g* for 30 min. The recovered supernatant was used to purify the GST-ZmFH polypeptides by batch affinity chromatography with glutathione sepharose 4B (GE Healthcare) incubating the mixture with gentle agitation for 60 min at room temperature. After three washes in PBS and, since the GST-ZmFH fusions include a thrombin recognition site, this protease was added (10 μg per mg of fusion protein) and digestion was carried out overnight at 20 °C. This allowed the separation of the GST fragment, which remained bound to the resin, from the fusion ZmFH proteins. After concentration using Centriprep Microcon 3 (Amicon, Merck, Darmstadt, Germany), proteins were finally purified through FPLC, in a gel filtration Superdex 75 column (GE Healthcare) equilibrated with 50 mM Tris-HCl, pH 7.0. The purified proteins were stored at −80 °C until further use.

2.7. Electrophoretic analyses of recombinant frataxins

The purified proteins were analyzed by 15% (w/v) PAGE [46], either with SDS (0.1% (w/v) final concentration, denaturing gels) or without SDS (native gels). Also, samples were analyzed both in normal and in reducing (*i.e.* 100 mM DTT final concentration) buffer. Total protein concentration was determined as described by Bradford [47].

2.8. ESI-MS of recombinant frataxins

Molecular mass determinations were performed by electrospray ionization time-of-flight mass spectrometry (ESI-TOF-MS). The equipment used was a Micro TOF-Q instrument (Bruker, Billerica, MA, USA) interfaced with an Agilent Series 1200 HPLC pump, both

controlled using the Compass Software. Calibration was attained with ESI-L Low Concentration Tuning Mix (Agilent Technologies, Santa Clara, CA, USA). All the samples were analyzed under the following conditions: 20 μL of protein solution injected at 40 μL min^{-1}; the capillary counter-electrode voltage was 5 kV; desolvation temperature about 90–110 °C. The carrier buffer was a 5:95 mixture of acetonitrile:ammonium acetate/ammonia (15 mM, pH 7.0).

2.9. Spectroscopic studies

Fluorescence spectra were recorded in a Varian Cary Eclipse, in an emission range of 305–450 nm, by exciting the samples at 295 nm. Frataxin samples were prepared by diluting the stock proteins to 3 μM with pH 7 Milli-Q water.

Circular dichroism (CD) spectra of frataxin samples were recorded using a Jasco J-815 spectropolarimeter equipped with a Peltier-controlled cell holder. Spectra were collected at 37 °C using a precision quartz cell of 2 mm path-length from 190 to 250 nm with a bandwidth of 1 nm and a scan speed of 100 nm/min. Frataxin samples were prepared by diluting the stock proteins to 0.5 μM with pH 7 Milli-Q water. Spectra were averaged over 5 scans and smoothed by Spectra Analysis (spectropolarimeter software). The secondary structure contents were derived by the CONTIN procedure [48] program Modified by Sreerama et al. [49]. The influence of O_2 on frataxin structures was studied by recording fluorescence and CD spectra on fresh samples and then, 24 h after incubation at 37 °C in aerobic conditions.

3. Results and discussion

3.1. Identification of Zea mays frataxin homologs and phylogenetic analysis

Using AtFH as the starting sequence, we searched for homologous maize genes in the Phytozome Database (https://phytozome.jgi.doe.gov/pz/portal.html). Thus, we identified two predicted *Zea mays* homologous genes that encode ZmFH-1 and ZmFH-2 proteins composed of 199 and 201 amino acids, respectively. These proteins share 72.9% of sequence identity. In addition ZmFH-1 and ZmFH-2 share 41.9 and 44.7% of sequence identity, respectively, with AtFH. It is important to note that maize is the first organism described that contains two genes coding for frataxin proteins. A blast search of several putative frataxin proteins from different plant species shows that, besides *Zea mays*, both *Glycine max* (soybean) and *Sorghum bicolor* also present more than one frataxin isoform (Fig. 1 A). The phylogenetic tree shows a clear distinction between monocotyledon and dicotyledon frataxins (Fig. 1 B) and it also reflects that frataxin duplication events may have happened more than once in plant evolution.

3.2. Homology modeling of ZmFH-1 and ZmFH-2

Two homology models of ZmFH-1 and ZmFH-2 were built using the 3D structure of the mature human frataxin (HF, PDB code 1EKG) [50]. Alignments of HF with ZmFH-1 and ZmFH-2 were performed using the HF main chain atoms of residues 90 to 208 (119 amino acids). The mature HF shares 40.9% of identity with residues 89–199 of ZmFH-1 and 38.6% identity with residues 90–201 of ZmFH-2. An alignment of the polypeptide backbone structure of HF with ZmFH-1 and ZmFH-2 showed that both 3D homology models are very similar among them and to HF (Fig. 2). Both models contain similar secondary structure elements, consisting of two alpha helices (α1-α2), five antiparallel segments forming a large beta sheet (β1-β5) and a second smaller beta sheet formed by the C-terminus of β5 and strands β6 and β7, as it has been reported for several frataxins, including those from *E. coli* [51], humans [50] and *Arabidopsis thaliana* [23]. Overall, all these secondary elements yield a set of very close 3D structures. Analysis using the Verify 3D program showed that 100% of the residues had an averaged 3D-1D score≥0.28 for ZmFH-2; whereas 99.08% of the residues had an averaged 3D-1D score≥0.2 for ZmFH-1, indicating that both models are of good quality.

Nevertheless, although both maize frataxins show a general 3D fold similar to HF, with highly conserved secondary structure elements, some differences are evident. First, the loop between helix α1 and the first strand of the beta sheet in both ZmFH-1 and ZmFH-2 it does not match with the HF one. The same thing occurs in the loops between strands β2 and β3, and β5 and β6 (Fig. 2D and E). These are non-conserved regions among frataxins from different taxa (Supplementary Fig. S1), that could explain the structural changes that probably affect their functions. Alternatively, these differences may represent specific adaptations of maize/plant frataxins to fulfill specific role/s in plant metabolism. The protein regions between helix α1 and the first strand of the beta sheet β1, and strands β2 and β3 are mostly conserved in plant frataxins (Fig. 1 A), and they tend to be close to the conserved C-terminal cysteine (Supplementary Fig. S2, see below presence of frataxin dimers).

Secondly, and more important, the maize frataxin C-terminal region extended from the α2 helix are shorter than in the human sequence (Fig. 2 A, B and C). The C-terminal region is a critical determinant of the fold and thermodynamic stability in the native protein [52], being both properties correlated with the length of the sequence and the network of interactions, with itself and with the rest of the protein, these amino acids establish. Most probably, maize frataxin foldings are less stable than HF (see below conformational changes), a fact that could impact in their function/s.

3.3. Expression of ZmFH genes in Zea mays

We analyzed the expression level of both ZmFH genes by RT-qPCR. Previous reports indicated that frataxin is predominantly expressed in tissues with high division rate and active mitochondrial energy metabolism. In mammals, frataxin is expressed mostly in liver, kidney and heart [1], while in *A. thaliana* plants was found mainly in flowers, but also expressed at lower levels in other tissues such as leaves and roots [23]. As shown in Fig. 3, both *ZmFH-1* and *ZmFH-2* are expressed in all maize plants tissues analyzed, confirming that both are functional genes. In agreement with previous data, high levels of frataxin transcripts were found in young developing tissues such as coleoptiles and young leaves, being *ZmFH-1* more expressed than *ZmFH-2*. This expression profile would reflect possible differences in the role of each gene *in vivo*.

3.4. Subcellular localization of ZmFH-1 and ZmFH-2

The predicted transit peptides for maize frataxin isoforms suggest mainly a mitochondrial localization. However, using different programs, we found that various algorithms also indicated a significant score for the targeting to chloroplasts for both proteins (Table 2).

To evaluate these predictions, we carried out the study of the cellular localization of ZmFH-1 and ZmFH-2. Thus, we transformed *A. thaliana* plants with plasmids coding for the predicted transit peptides from both proteins fused to green fluorescent protein DNA coding sequence under the control of the constitutive CaMV35S promoter. Then, we have isolated protoplasts from the selected plants and search for GFP location using fluorescent confocal microscopy. Results showed that ZmFH-1TP-GFP colocalized with the red fluorescence signal corresponding to the mitochondrial marker,

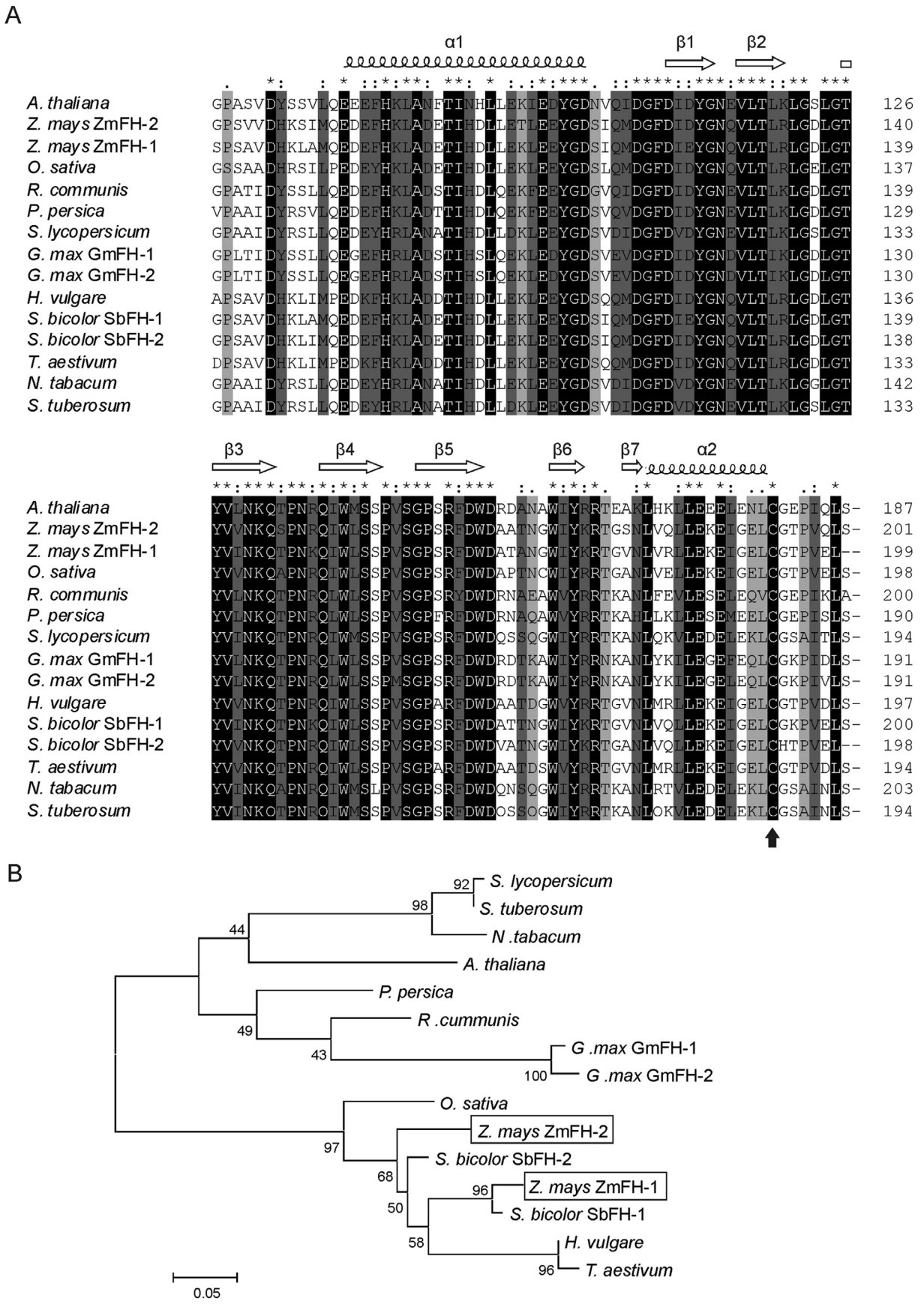

Fig. 1. Bioinformatics studies of frataxin homologous in plants. (**A**) Multiple amino acid sequence alignment of frataxin domain from different species. Alignment was performed by using the Clustal X2 method. The amino acid sequence, without the N-terminus residues, of *Arabidopsis thaliana* (accession number AT4G03240.1) is compared with those

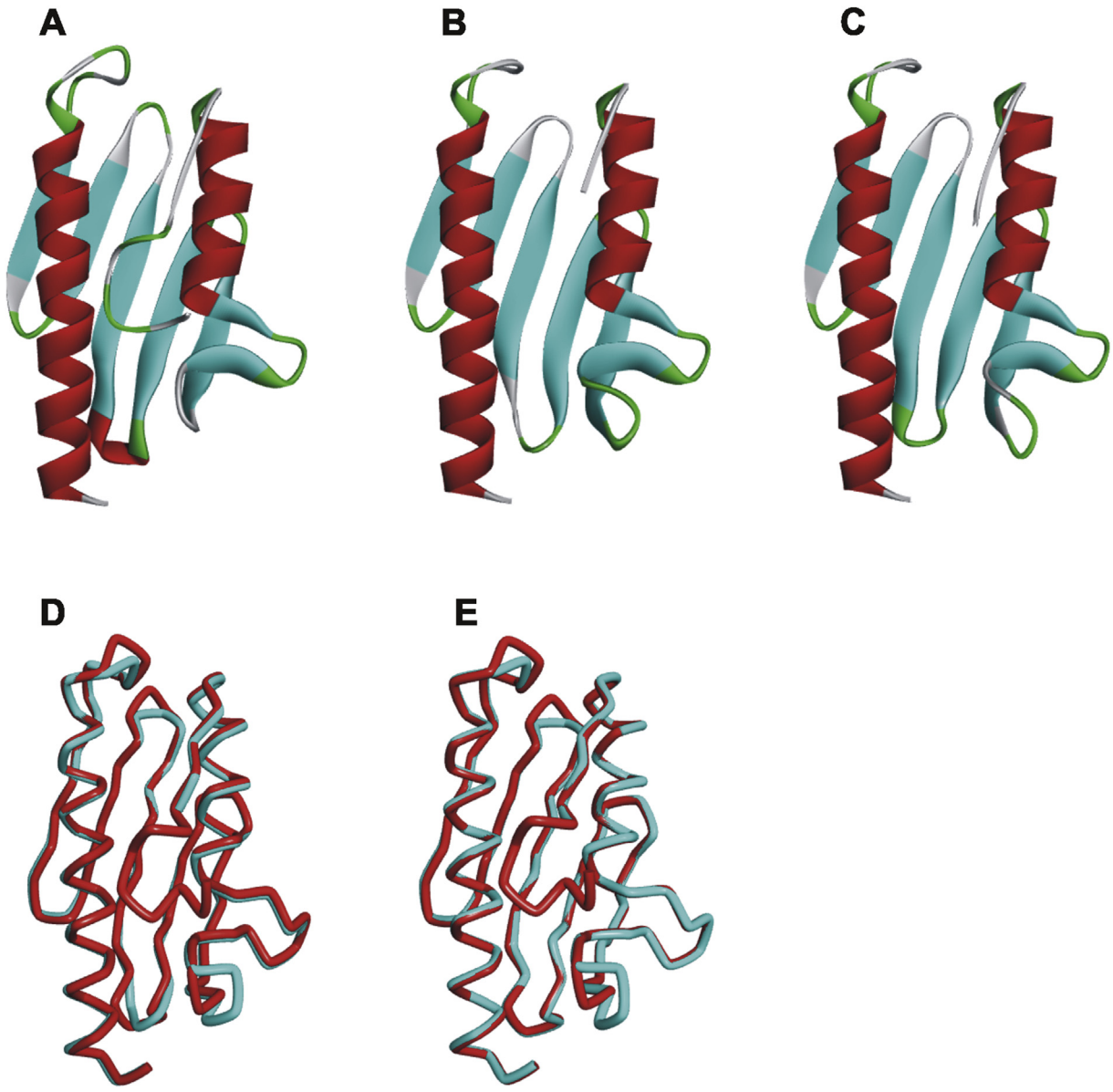

Fig. 2. 3D homology model of mature ZmFH-1 and ZmFH-2. Ribbon structures showing the fold of Human frataxin (HF, PDB ID 1EKG) (**A**) and the homology models of ZmFH-1 (**B**) and ZmFH-2 (**C**). α helices are colored in red, β strands are represented in cyan and β turns are indicated in green. (**D**) and (**E**) show the superposition of the 1EKG HF 3D structure (red tube) with the homology models of ZmFH-1 (**D**) and ZmFh-2 (**E**), both colored in cyan.

whereas ZmFH-2TP-GFP show a fluorescence pattern that colocalized with both mitotraker and chlorophyll autofluorescence, indicating a dual localization in mitochondria and chloroplasts (Fig. 4 A).

To further confirm these results, we also performed the localization studies in *N. benthamiana* infiltrated leaves. The fluorescence patterns indicate a significant accumulation of ZmFH-1TP-GFP and ZmFH-2TP-GFP in both, mitochondria and chloroplasts, suggesting a dual localization in both plant organelles (Fig. 4 B).

Our results imply that at least one maize frataxin isoform would be present in both chloroplasts and mitochondria. This could be explained by the amino acid composition of both Zm-FH transit peptides. They are enriched in hydrophobic and positively charged residues, and significantly deficient in acidic residues, similar to other ambiguous targeting proteins reported [53]. Moreover, this is in concordance with many reported proteins with mitochondrial predicted targeting signals that finally present dual localization, perhaps due to ambiguous transit peptides, which interact with

corresponding to *Zea mays*, ZmFH-1 and ZmFH-2 (accession number GRMZM2G062342 and GRMZM2G083755), *Oryza sativa* (accession number Os01g57460.1), *Ricinus communis* (accession number XP_002531340.1), *Prunus persica* (accession number ppa011940m), *Solanum lycopersicum* (accession number Solyc07g053150.2.1), *Glycine max* (accession number Glyma19g29700.1 −GmFH-1- and Glyma03g00960.1 −GmFH-2), *Hordeum vulgare* (accession number BAK02524.1), *Sorghum bicolor* (accession number sobic.007G212800.1 −SbFH-1- and sobic.003G319100.1 −SbFH-2), *Triticum aestivum* (accession number CDM84506.1), *Nicotiana tabacum* (accession number XP_016433288.1) and *Solanum tuberosum* (accession number XP_006360538.1). Identical residues (*) are marked in black and conserved substitutions (:) are shaded in gray. The black arrow indicates the conserved plant cysteine. (**B**) Molecular Phylogenetic analysis of frataxin from different species. The phylogenetic tree was constructed with frataxin protein sequences from several plants species using the Maximum Likelihood method in MEGA5 software. Maize frataxin are boxed. Bootstrap values from 1000 replicates were indicated at each branch.

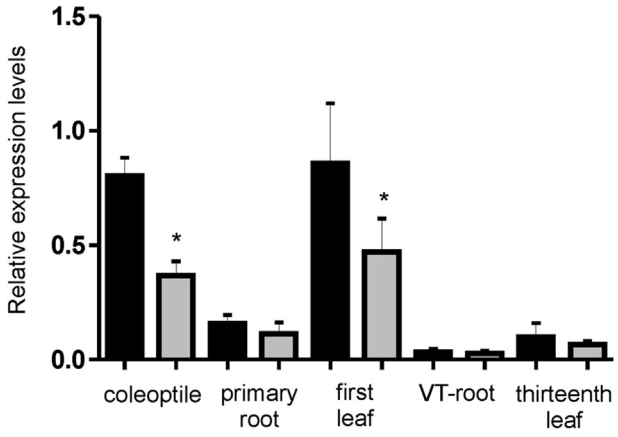

Fig. 3. Transcript expression profiles of maize frataxin isoforms in different plant tissues. *ZmFH-1*and *ZmFH-2* transcript levels, relative to actin values, were determined by RT-qPCR in wild-type maize plants in the following tissues: coleoptile, V1-primary root, V1-first leaf, VT-root and VT-thirteenth leaf. (V1: vegetative stage-1, VT: tasseling stage in maize development). Bars represent mean values ± standard deviation. The black bars indicate *ZmFH-1*, and the gray ones correspond to *ZmFH-2*. The asterisk denotes a statistically different result between both frataxin isoforms in each tissue ($P < 0.05$).

Table 2
Score prediction of mitochondrial and chloroplast localization of ZmFH-1 and ZmFH-2, with the bioinformatics tools: GTP_pp, GTP_ref, TargetP, Mitoprot, ChloroP y Predotar [33,42,43].

Program	Mitochondria	Chloroplast
ZmFH-1		
GTP_pp	0.765	0.503
GTP_ref	0.418	0.594
Target P	0.938	0.349
Mitoprot	0.964	–
ChloroP	–	0.566
Predotar	0.87	0.10
ZmFH-2		
GTP_pp	0.691	0.239
GTP_ref	0.388	0.622
Target P	0.714	0.152
Mitoprot	0.998	–
ChloroP	–	0.522
Predotar	0.57	0.09

both organelle protein transport machinery [54].

We have recently shown that in *A. thaliana* frataxin is encoded by a single gene and the protein is located in mitochondria and chloroplasts [31]. Our data suggest that AtFH would play a major role in plant Fe-S metabolism in both organelles since its deficiency alters the biological activity of several mitochondrial and chloroplasts Fe-S proteins [9,31]. Thus, it is possible that each ZmFH protein plays a similar role in chloroplasts and mitochondria as occurs with AtFH, participating in the normal functioning of the photosynthetic electron transport chain in chloroplasts and regulating the Fe-S biosynthesis and iron metabolism in both organelles [31].

3.5. Complementation of Saccharomyces cerevisiae

It has been reported previously that frataxin knockout yeasts are hypersensitive to oxidants as demonstrated by their sensitivity to hydrogen peroxide [3]. To study the function of ZmFH-1 and ZmFH-2, we evaluated the ability of these proteins to restore the normal phenotype of frataxin knockout yeast (*Δyfh*) when it is complemented with maize frataxin isoforms. Thus, *Δyfh* cells alone or complemented with each isoform were treated with 2 mM H_2O_2 and then transferred to complete YP-galactose medium. The null mutant shows a lower growth rate and a higher sensitivity to hydrogen peroxide than the wild type cells. In contrast, the complemented yeast cells showed an increased resistance to oxidative stress (Fig. 5). Cells expressing ZmFH-1 grew until the fourth dilution after H_2O_2 treatment indicating that this isoform is more efficient than ZmFH-2 –which also grew until the fourth dilution but much less vigorously- to restore the phenotype. As it was described for AtFH [23], these results point to a protective role against oxidants for these isoforms and suggest that both ZmFH proteins may have different relevance in the protection against oxidative damage.

3.6. Heterologous expression in E. coli cells and purification of ZmFH-1 and ZmFH-2

DNA sequencing of the insertions in the pGEX–ZmFH-1 and pGEX–ZmFH-2 confirmed the correct in-frame ligation of the respective ZmFH cDNAs into the GST coding portion, as well as the absence of undesired mutations. Furthermore, total protein extracts of IPTG-induced *E. coli* BL21 cultures revealed the presence of GST-ZmFH fusions of the expected size for each cloned cDNAs (data not shown).

Synthesis at small scale (*i.e.* 5 l of culture grown in several 2 l Erlenmeyer flasks) of ZmFH-1 and ZmFH-2 invariably rendered one peak of protein in the last FPLC purification step (Fig. 6 A). This peak was identified by ESI-MS and SDS-PAGE (Fig. 6 A, B) as the expected ZmFH monomer (plus the N-terminal GS residues resulting from the thrombin digestion of the GST-fusion proteins). Hence, ESI-MS of purified ZmFH-1 and ZmFH-2, run both at neutral and acid pH, exhibit major peaks of 14612 and 14416 Da, respectively (Fig. 6 B). The expected MM of recombinant ZmFH-1 and ZmFH-2 are 14613.2 and 14416.0 Da, respectively. These results confirmed that synthesized protein monomers were devoid of metal ions. Only minor peaks of MM compatible with protein dimers were detected (experimental MM of 29226 for ZmFH-1 and 28832 for ZmFH-2, exactly matching the theoretical values). The presence of dimers was also apparent when samples were analyzed by native PAGE. Hence, a monomeric band accompanied with a band with a molecular mass matching that of the protein dimers, especially for ZmFH-2, is evident from Fig. 6C. Interestingly, the bands corresponding to the dimeric species are fully eliminated by addition of the reducing agent DTT, which suggested that the dimers result from the monomer oxidation. In this sense, it is quite striking that both ZmFH-1 and ZmFH-2, in contrast to frataxins from other kingdoms (Fig. S1), contain one cysteine in their C-terminal amino acid sequence [23]. The Cys residues, located at position 193 and 194 for ZmFH-1 and ZmFH-2, respectively, could be involved in the oxidation of proteins, with the subsequent formation of the disulfide bond, which could justify the presence of dimers and the restoration to monomers by DTT. It is interesting to note that this C-terminal Cys residue is well conserved in most plant frataxins, such as those from *A. thaliana*, *T. aestivum* and *O. sativa,* among others, at positions 180, 187 and 191, respectively, suggesting that this residue could be critical for the function of frataxin in photosynthetic organisms (Fig. 1 A). Cysteine is one of the least abundant amino acids in the proteome [55]. Nevertheless, when they are present and conserved, cysteine residues tend to have a relevant role in the function of the protein. Being highly reactive, they are usually buried in the hydrophobic core of a protein as part of catalytic sites, or located on the surface exposed to the solvent acting as switch sensors [56]. There are many examples of proteins whose solvent exposed cysteines suffer modifications leading to a change in activity or other functional properties of the protein, like the

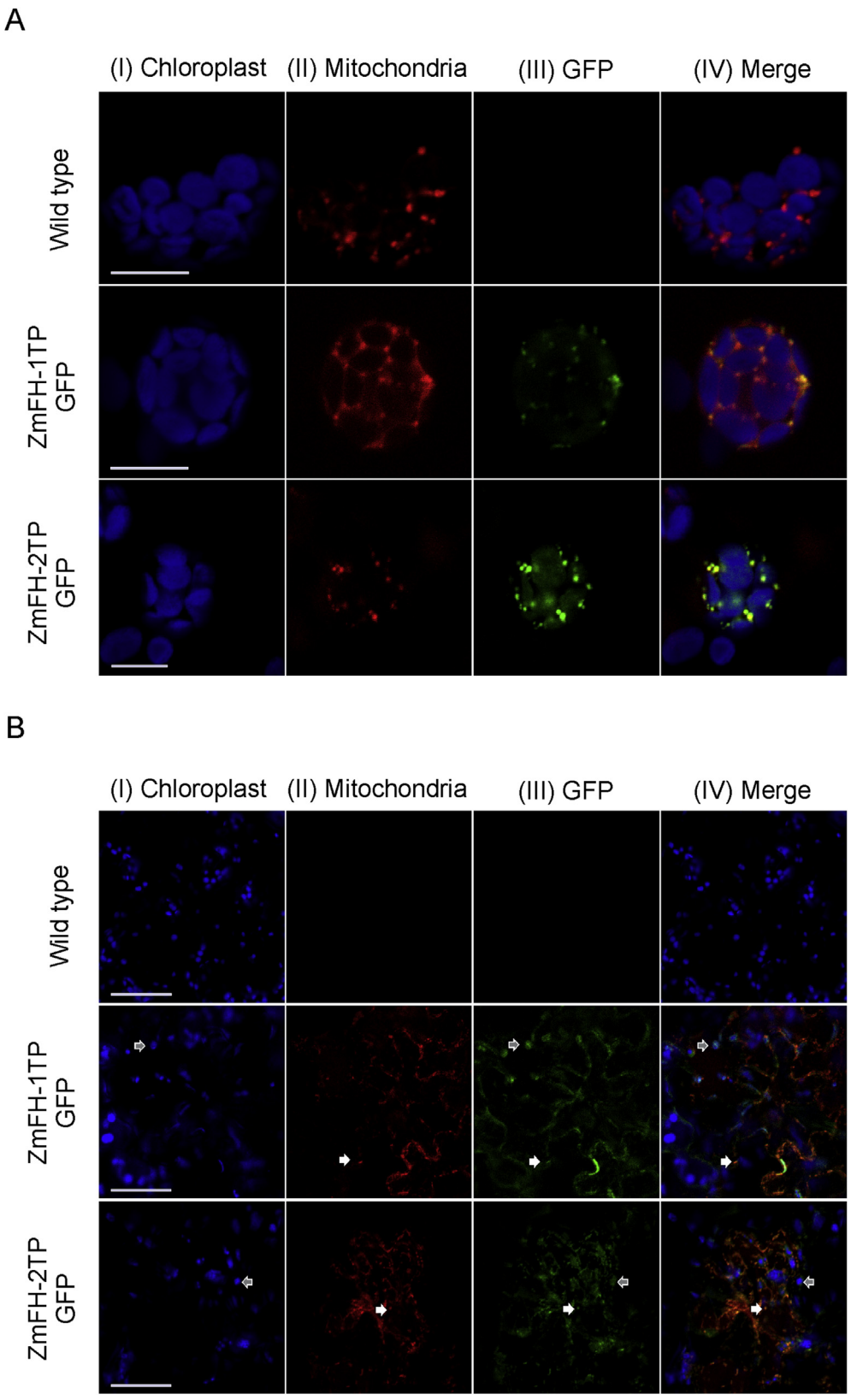

Fig. 4. Subcellular localization of maize frataxin isoforms in heterologous systems. (**A**) Localization studies in *Arabidopsis thaliana* protoplasts. The plasmids pZP212 containing the peptide transit coding sequences *ZmFH-1TP* and *ZmFH-2TP*, fused to GFP, were introduced into *A. thaliana* Col-0 plants by the floral dip method. Protoplasts isolated from wild-type and transgenic plants were analyzed by fluorescence confocal microscopy. Fluorescence is shown from (I) Chlorophyll autofluorescence (excitation 488 nm/emission 650 nm); (II) Mitotracker staining (excitation 543 nm/emission 576 nm); (III) GFP fluorescence (excitation 488 nm/emission 510 nm); (IV) Overlay of I, II and III, showing coincidence of GFP localization with markers. Scale: 10 μm. (**B**) Subcellular localization in *Nicotiana benthamiana* leaves. Confocal microscopy images were acquired from leaves of wild-type plants, leaves infiltrated with pZP212. ZmFH-1TP-GFP, and leaves infiltrated with pZP212. ZmFH-2TP-GFP. Fluorescence is shown from (I) Chlorophyll autofluorescence (excitation 488 nm/emission 650 nm); (II) mCherry mitochondrial marker (excitation 543 nm/emission 576 nm); (III) GFP fluorescence (excitation 488 nm/emission 510 nm); (IV) Overlay of I, II and III, showing coincidence of GFP localization with markers. The white arrows indicate co-localization with mitochondria and the gray ones indicate co-localization with chloroplast. Scale: 50 μm.

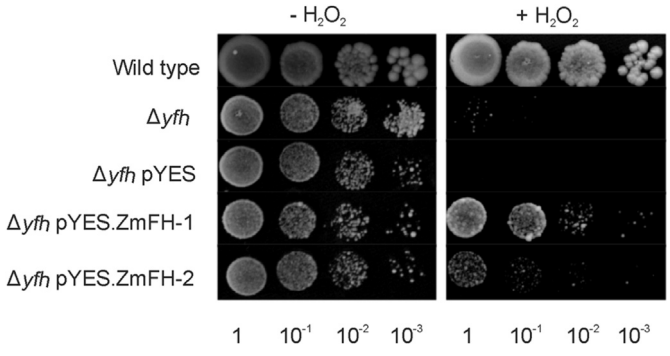

Fig. 5. Complementation of YFH deficiency by ZmFH-1 and ZmFH-2. The sensitivity of wild-type *S. cerevisiae* DY150, *Δyfh* and Δ*yfh* transformed with pYES, pYES.ZmFH-1 and pYES.ZmFH-2 cells to oxidative damage were evaluated after treatment with H_2O_2. Yeasts were incubated in 2 mM H_2O_2 for 60 min and 3 μl of each culture serial dilutions were spotted on YP 2% (w/v) Galactose medium. Photographs were taken after 3 days of growth at 30 °C.

prokaryotic OxyR [57] or the *S. cerevisiae* YAP1 [58] transcription factors. This could also be the case of plant frataxins.

3.7. Aggregation and conformational studies of ZmFH-1 and ZmFH-2

A commonly reported feature of all known frataxins is their ability to assemble, which is probably related to the dynamism of their structures [20]. Here, ZmFH aggregation and/or conformational changes were analyzed, taking the recombinant ZmFH-2 isoform as a model, through i) the analysis of its spontaneous trend (*i.e.* intrinsic, non metal-driven) of undergoing polymerization or ii) input of an external chemical signal, such as O_2 presence (*i.e.* open air incubation).

To this end, synthesis of ZmFH-2 was repeated in large-scale conditions in a 10 l fermenter equipped with temperature, O_2 and pH controllers. Strikingly, in this case, two well-resolved FPLC peaks were obtained, in contrast with the single peak achieved in Erlenmeyer productions (about 500–1000 ml, Fig. 7 A). The native PAGE of the first peak revealed a very high molecular weight band, a faint band at 60 kDa and the total absence of monomer (Fig. 7 B). The HMM-ZmFH-2 species was sensible to SDS (Fig. 7 B) in accordance with its polymeric nature. It is worth noting that the only distinct bands in denaturing conditions, besides the monomer running with the front, indicate aggregates of 60 and 90 kDa, which would correspond to tetramers and hexamers of ZmFH-2. However, ESI-MS analysis of this sample only yielded a ZmFH-2 monomeric peak, indicating that either the MS running conditions were too harsh to maintain the aggregated state, or that the high molecular mass species formed was unable to be ionized and then detected by ESI-MS. In any case, the monomer observed by ESI–MS would be the result of the disaggregation from the HMM polymer or just the small remaining fraction of a monomer capable of being ionized, in agreement with the low intensity of the peak. In contrast, the second FPLC peak mainly contained monomeric ZmFH-2, showing similar features by ESI-MS to those displayed by the sample recovered from small-scale cultures (see Fig. 6 B and 7C). These findings clearly evidence that culture conditions can lead to aggregation of frataxins as despite monomeric species are also recovered, an important part of the synthesized protein is in an HMM aggregated state, as reported for the HF.

Subsequently, and in order to investigate if the possible origin of the distinct aggregation states of frataxin found both in the small- (dimers) and in the large-scale (HMM polymers) productions of ZmFH-2 (Fig. 6C and 7 B) was due to an airborne sample oxidation, ZmFH-2 samples were left in open air for several hours, and then analyzed by native PAGE and ESI-MS (Fig. 8). PAGE revealed that air exposure did not lead to dimer formation but to the appearance of a novel monomeric band (named from now on monomer β) of slight faster mobility than the original monomer (named from now on monomer α) (Fig. 8 A). ESI-MS spectra of both (fresh & oxygenated) samples shared the same peaks and therefore the same molecular weight (Fig. 8 B), evidencing that α and β are two distinct conformations of the same monomeric protein. Therefore, the most plausible explanation for this experimental data is to assume that O_2 provokes a conformational change from the α to the β monomer, which shows different electrophoretic mobility in native gels.

The possible O_2-driven transformation from α-type to β-type monomer was monitored by fluorescence, UV–Vis and CD spectroscopies. Remarkably, the auto-fluorescence of the α-monomer displays a maximum at 350 nm that moves to 390 nm when exposed 24 h to open air (Fig. 8C). A similar behavior was observed for the other maize frataxin analyzed in this work (ZmFH-1). Protein fluorescence at 350 nm is usually attributable to buried tryptophan residues, and the change to 390 nm would reveal an alteration of the Trp microenvironment leading to a more exposed state [59], compatible with the alleged protein conformational change. Both ZmFH studied polypeptides harbor three Trp residues in its C-terminal region that could perfectly account for this phenomenon. Nevertheless the Trp 153 lateral chain is already exposed in the ZmFH-2 3D model –projecting outside the plane defined by the β-sheet (Fig. 8 E). This could be the reason wht change in protein fluorescence maximum may be attributed to the exposure of Trp 166 and Trp 173, the Trp residues whose indole side chains are buried in the protein core. It has been shown that yeast frataxin interacts with Isu1 through Trp 131 [60], and conserved and exposed Trp are preferential protein–protein interaction hot spots [61]. Indeed, Trp 166 and 173 are conserved in all plant frataxins (Fig. 1 A). So this phenomenon of conformational change from monomer α to monomer β with the exposure of additional Trp residues might be relevant for the interaction of plant frataxins with proteins of the [Fe-S] cluster biosynthetic pathways, or other pathways, in physiological conditions where oxygen is abundant.

Likewise, the CD spectra of ZmFH-1 and ZmFH-2 after incubation at 24 h in aerobiosis showed significant differences on those of freshly samples (Fig. 8 D). The experimental CD spectra fitted with CONTIN correspond to a mixture of frataxins with different structures. Air exposure produces an increase of β-strand in detriment of the α-helix structure. Thus, whereas the CD spectrum of the α-ZmFH-2 monomer (fresh sample) matches a 13% of α-helix and a 33% of β-strand, that of the air exposed sample (including both α-ZmFH-2 and β-ZmFH-2 monomers reaches 40% of β-strand and lowers to a 6% of α-helix (Fig. 8 D). The increase of β-strand in a protein leads to a bigger exposure of its structure. Therefore, both the progress of the fluorescence and that of the CD spectra, together with the invariability of the ESI-MS spectra accompanying these spectroscopic changes, from the fresh to the aerated sample suggest the existence of a conformational change from a monomer a-ZmFH-2 to a monomer b-ZmFH-2, the latter with a more open structure. This is also supported by the structural features of the 3D model, with the short C-terminal extension imparting low thermodynamic stability to the fold [52].

Interestingly, the role of O_2 in these processes is not that of an oxidant, since the addition of common oxidants, such as metal ions or H_2O_2, induces other kinds of structural changes, in particular, the formation of disulfide-bridged dimers by cysteine oxidation (data not shown, manuscript in preparation). Studies to decipher the physiological significance of the oxygen driven conformational changes are on the way.

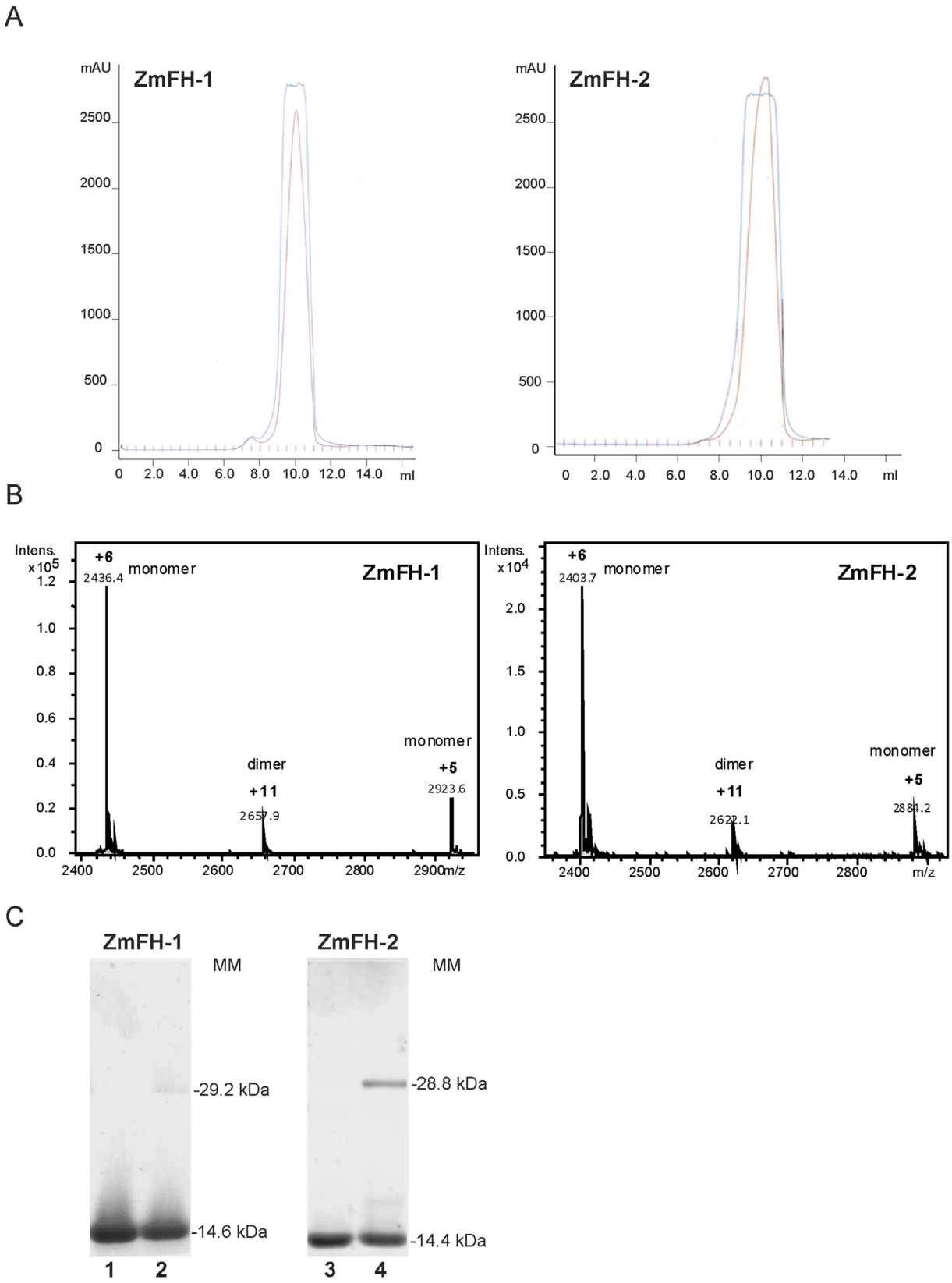

Fig. 6. Expression and purification of recombinant ZmFH-1 and ZmFH-2. (**A**) Superdex 75 FPLC spectra of Erlenmeyer-scale syntheses (about 500–1000 ml), (**B**) ESI-MS and (**C**) Native PAGE analysis of the ZmFH-1(left) and ZmFH-2 (right) recombinant proteins. Blue and red lines in (A) correspond to 280 and 254 nm, respectively. Lanes in (C) correspond to: (1) ZmFH-1 with DTT; (2) ZmFH-1 w/o DTT; (3) ZmFH-2 with DTT; and (4) ZmFH-2 w/o DTT in sample buffer.

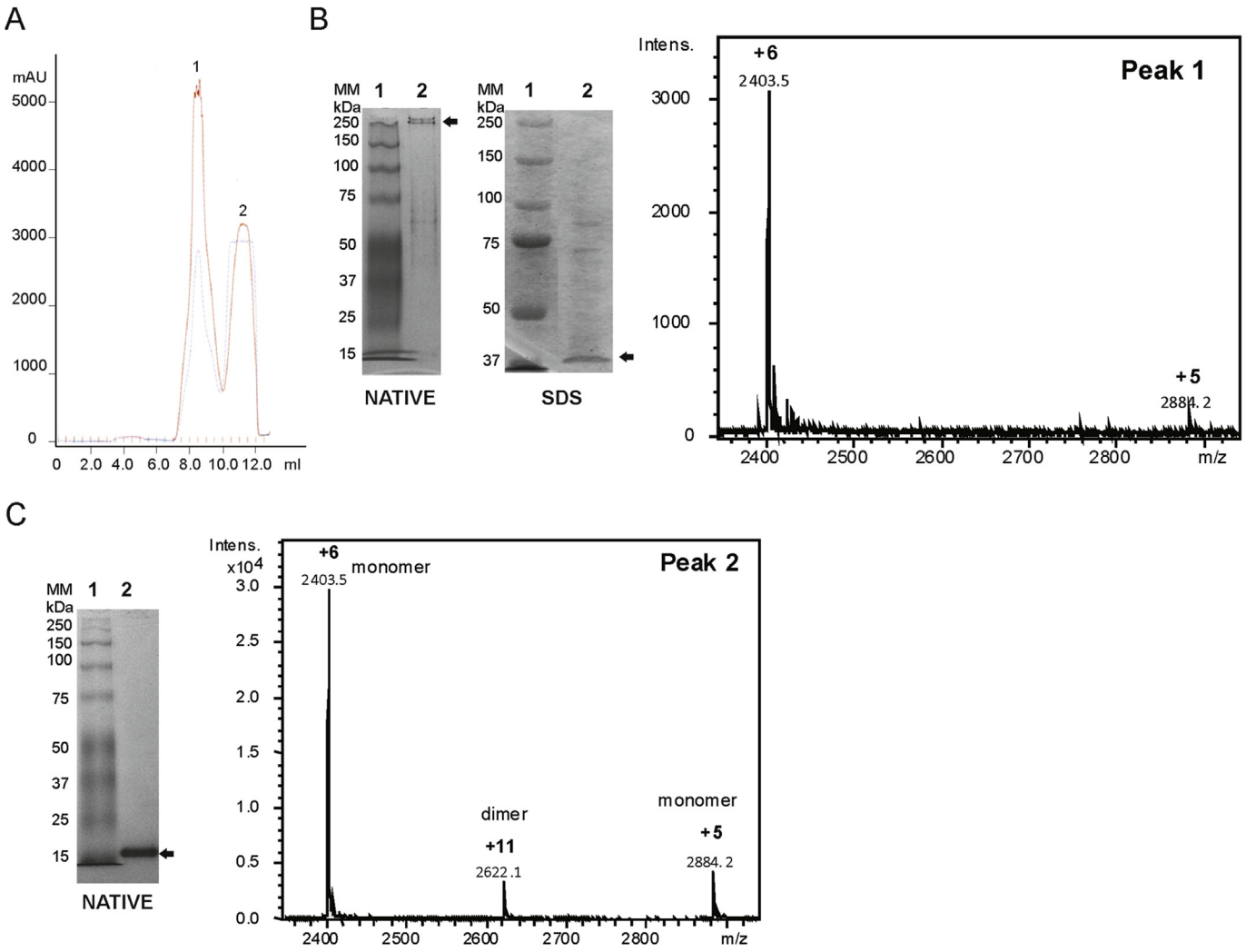

Fig. 7. Fermenter-scale syntheses of ZmFH-2. (**A**) Superdex 75 FPLC spectra of ZmFH-2. Blue and red lines in correspond to 280 and 254 nm, respectively. Native PAGE and ESI-MS analysis of peak 1 (**B**) and peak 2 (**C**). Lanes 1 and 2 in each gel correspond to molecular weight markers (MWM) and the analyzed sample, respectively. In the native gels, the MM are just indicative.

4. Conclusions

This is the first study of a plant that hosts two frataxin isoforms coded in its genome. Both proteins have a high identity and similar structure respect to other frataxin homologs like AtFH or HF. This is also reflected by the high-quality homology models of their 3D structure using the mature HF as a scaffold, showing the characteristic secondary structure elements of the family. Moreover, the functional conservation was validated by the phenotypic rescue of yeast frataxin knockout mutants under oxidative stress.

ZmFH-1 and *ZmFH-2* are functional genes, expressed in all the maize tissues studied. Their transcript levels were highest in young developing tissues, pointing that the protein function/s might be related to the energy producing pathways and organelles. Due to the mitochondrial location of this protein in non-photosynthetic eukaryotes, it was reported that frataxin deficiency causes changes in the function of the organelle [6,62]. As we recently reported for *A. thaliana* plants [31], here we also show that both *Zea mays* frataxin isoforms are located in mitochondria and chloroplasts. Chloroplasts contain a SUF-type machinery for the synthesis of their Fe-S proteins. This system is similar to the ISC found in mitochondria, having both systems homologous proteins [63,64]. It is possible that plant frataxins play similar roles in the two organelles, either as iron donors, modulating the activity of the ISC and SUF systems —regulating the activity of proteins involved in the pathways- or in a yet to be discovered new function.

Aggregation and conformational studies of frataxins have been previously carried out in protein samples obtained by heterologous *E. coli* synthesis of yeast, bacteria and human frataxin homologs. Recombinant productions of both ZmFH-1 and ZmFH-2 at small-scale always render apo-monomer, with a modest presence of the corresponding dimers. However, the syntheses of these frataxins on a fermenter scale yield two pools of protein, one of a high molecular weight (HMM) and the other containing an apo-monomer with the same features than the apo-monomer obtained by Erlenmeyer cultures. The HMM aggregates are not detectable by ESI-MS but are clearly seen by native PAGE, accompanied by traces of hexamers and tetramers. The exposure of both ZmFH-1 and ZmFH-2 monomers (the so-called α-monomers) to aerobiosis for 24 h causes a conformational change to a partially unfolded state (the so-called β-monomer), this shown by PAGE, CD and fluorescence results and supported by the C-terminal features of the 3D homology models.

All these features match the following behaviors reported in the

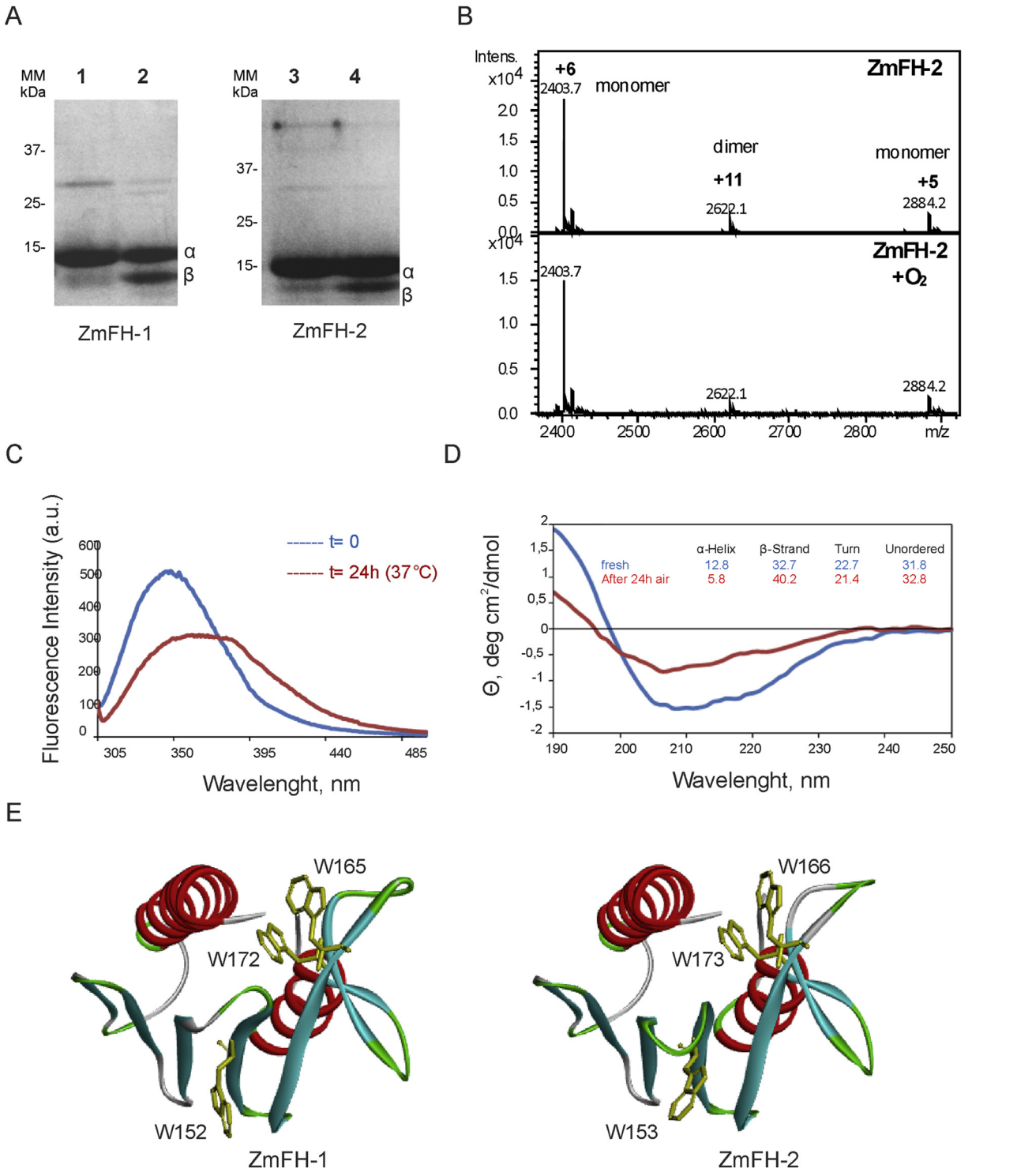

Fig. 8. Effect of air exposure on maize frataxins. (**A**) Native PAGE gels of ZmFHs samples left in open air. Lanes 1 and 3 are freshly purified ZmFH-1 and ZmFH-2 proteins. Lanes 2 and 4 are the proteins after 1 day of exposure at 37 °C to open air (**B**) ESI-MS analysis of ZmFH-2 before and after exposure to open air. (**C**) Autofluorescence and (**D**) Circular Dichroism of ZmFH-2 samples before and after 24 h of exposure to open air. The inserted Table shows the percentage of the secondary structure elements in each case. (**E**) 3D model of ZmFH-2 showing the lateral chain orientation of its three Trp amino acid residues.

literature for the other recombinantly studied frataxin family proteins. Hence yeast YFH1, as *E. coli* CyaY, does not aggregate *in vivo*, and remarkably the multimers formed by *in vitro* iron addition are never detected by ESI-MS [22,65] probably because, as explained before, either the MS running conditions are too harsh to maintain the aggregated state, or the high molecular weight species formed are unable to be ionized and then detected by ESI-MS. In contrast, HF is produced as two forms, one soluble monomer and an HMM fraction, which is never detected by ESI-MS. 30% of the HF monomer never assemblies -maybe the protein fold is incompatible with self assembly-, and only 70% of the total recombinant HF maintains this capability. Therefore the HF aggregates *in vivo*, but it does it

poorly *in vitro* even in the presence of metal (iron) [66]. Further studies on the nature of plant frataxin homolog oxidation, dimerization, oligomerization and interaction with metal ions are in the way.

Author contributions

DFGC, MAP, SA and JMDV planned experiments, CB, MS, MCar and OP performed experiments, CB, MS, MCap and MVB analyzed data and DFGC, MAP, SA and MCap wrote the paper.

In memoriam

This work is dedicated to the memory of Professor Dr. Silvia Atrian who passed away in December 2016. We had the good fortune to know Silvia and planned and discussed many scientific experiments. We wish to dedicate this work to her as a sign of immense regard for our colleague and friend.

Acknowledgements

This work was generously supported by Agencia Nacional de Promoción Científica y Técnica (Argentina), PICT 2013-2188, 2014-2184 and 2016-0350 (to DFGC) and by the Spanish Ministerio de Economía y Competitividad (MINECO), grants CTQ2015-70371-REDT (all Spanish authors), CTQ2015-64538-R (to JMD-V), BIO2015-67358-C2-1-P (to SA) and -C2-2-P (to MC), which are co-financed by the European Union through the FEDER program. SA, MC, and OP are members of the 2014SGR-423 Grup de Recerca de la Generalitat de Catalunya. Experimental support of Dra. E. Jiménez is greatly appreciated. We thank the Centres Científics i Tecnològics (CCiT) de la Universitat de Barcelona (ICP-AES, DNA sequencing) and the Servei d'Anàlisi Química (SAQ) de la Universitat Autònoma de Barcelona (CD, UV–vis, ESI-MS) for allocating instrument time. MVB, MAP and DFGC are researchers from CONICET, Argentina.

Appendix A. Supplementary data

Supplementary data related to this article can be found at http://dx.doi.org/10.1016/j.biochi.2017.06.011.

References

[1] H. Koutnikova, V. Campuzano, F. Foury, P. Dolle, O. Cazzalini, M. Koenig, Studies of human, mouse and yeast homologues indicate a mitochondrial function for frataxin, Nat. Genet. 16 (4) (1997) 345–351.
[2] V. Campuzano, L. Montermini, Y. Lutz, L. Cova, C. Hindelang, S. Jiralerspong, Y. Trottier, S.J. Kish, B. Faucheux, P. Trouillas, F.J. Authier, A. Durr, J.L. Mandel, A. Vescovi, M. Pandolfo, M. Koenig, Frataxin is reduced in Friedreich ataxia patients and is associated with mitochondrial membranes, Hum. Mol. Genet. 6 (11) (1997) 1771–1780.
[3] M. Babcock, D. de Silva, R. Oaks, S. Davis-Kaplan, S. Jiralerspong, L. Montermini, M. Pandolfo, J. Kaplan, Regulation of mitochondrial iron accumulation by Yfh1p, a putative homolog of frataxin, Science 276 (5319) (1997) 1709–1712.
[4] G. Isaya, H.A. O'Neill, O. Gakh, S. Park, R. Mantcheva, S.M. Mooney, Functional studies of frataxin, Acta Paediatr. Suppl. 93 (445) (2004) 68–71 discussion 72–3.
[5] F. Prischi, P.V. Konarev, C. Iannuzzi, C. Pastore, S. Adinolfi, S.R. Martin, D.I. Svergun, A. Pastore, Structural bases for the interaction of frataxin with the central components of iron-sulphur cluster assembly, Nat. Commun. 1 (2010) 95.
[6] M.V. Busi, D.F. Gomez-Casati, Exploring frataxin function, IUBMB Life 64 (1) (2012) 56–63.
[7] U. Muhlenhoff, N. Richhardt, M. Ristow, G. Kispal, R. Lill, The yeast frataxin homolog Yfh1p plays a specific role in the maturation of cellular Fe/S proteins, Hum. Mol. Genet. 11 (17) (2002) 2025–2036.
[8] O.S. Chen, S. Hemenway, J. Kaplan, Inhibition of Fe-S cluster biosynthesis decreases mitochondrial iron export: evidence that Yfh1p affects Fe-S cluster synthesis, Proc. Natl. Acad. Sci. U. S. A 99 (19) (2002) 12321–12326.
[9] M.V. Busi, M.V. Maliandi, H. Valdez, M. Clemente, E.J. Zabaleta, A. Araya, D.F. Gomez-Casati, Deficiency of Arabidopsis thaliana frataxin alters activity of mitochondrial Fe-S proteins and induces oxidative stress, Plant J. 48 (6) (2006) 873–882.
[10] M. Ristow, M.F. Pfister, A.J. Yee, M. Schubert, L. Michael, C.Y. Zhang, K. Ueki, M.D. Michael 2nd, B.B. Lowell, C.R. Kahn, Frataxin activates mitochondrial energy conversion and oxidative phosphorylation, Proc. Natl. Acad. Sci. U. S. A 97 (22) (2000) 12239–12243.
[11] A. Martelli, H. Puccio, Dysregulation of cellular iron metabolism in Friedreich ataxia: from primary iron-sulfur cluster deficit to mitochondrial iron accumulation, Front. Pharmacol. 5 (2014) 130.
[12] S. Park, O. Gakh, H.A. O'Neill, A. Mangravita, H. Nichol, G.C. Ferreira, G. Isaya, Yeast frataxin sequentially chaperones and stores iron by coupling protein assembly with iron oxidation, J. Biol. Chem. 278 (33) (2003) 31340–31351.
[13] A.L. Bulteau, H.A. O'Neill, M.C. Kennedy, M. Ikeda-Saito, G. Isaya, L.I. Szweda, Frataxin acts as an iron chaperone protein to modulate mitochondrial aconitase activity, Science 305 (5681) (2004) 242–245.
[14] E. Lesuisse, R. Santos, B.F. Matzanke, S.A. Knight, J.M. Camadro, A. Dancis, Iron use for haeme synthesis is under control of the yeast frataxin homologue (Yfh1), Hum. Mol. Genet. 12 (8) (2003) 879–889.
[15] M.V. Maliandi, M.V. Busi, V.R. Turowski, L. Leaden, A. Araya, D.F. Gomez-Casati, The mitochondrial protein frataxin is essential for heme biosynthesis in plants, FEBS J. 278 (3) (2011) 470–481.
[16] R.A. Schoenfeld, E. Napoli, A. Wong, S. Zhan, L. Reutenauer, D. Morin, A.R. Buckpitt, F. Taroni, B. Lonnerdal, M. Ristow, H. Puccio, G.A. Cortopassi, Frataxin deficiency alters heme pathway transcripts and decreases mitochondrial heme metabolites in mammalian cells, Hum. Mol. Genet. 14 (24) (2005) 3787–3799.
[17] O. Gakh, S. Park, G. Liu, L. Macomber, J.A. Imlay, G.C. Ferreira, G. Isaya, Mitochondrial iron detoxification is a primary function of frataxin that limits oxidative damage and preserves cell longevity, Hum. Mol. Genet. 15 (3) (2006) 467–479.
[18] H.A. O'Neill, O. Gakh, S. Park, J. Cui, S.M. Mooney, M. Sampson, G.C. Ferreira, G. Isaya, Assembly of human frataxin is a mechanism for detoxifying redox-active iron, Biochemistry 44 (2) (2005) 537–545.
[19] S. Park, O. Gakh, S.M. Mooney, G. Isaya, The ferroxidase activity of yeast frataxin, J. Biol. Chem. 277 (41) (2002) 38589–38595.
[20] K.Z. Bencze, K.C. Kondapalli, J.D. Cook, S. McMahon, C. Millan-Pacheco, N. Pastor, T.L. Stemmler, The structure and function of frataxin, Crit. Rev. Biochem. Mol. Biol. 41 (5) (2006) 269–291.
[21] A. Pastore, H. Puccio, Frataxin: a protein in search for a function, J. Neurochem. 126 (Suppl 1) (2013) 43–52.
[22] S. Adinolfi, M. Trifuoggi, A.S. Politou, S. Martin, A. Pastore, A structural approach to understanding the iron-binding properties of phylogenetically different frataxins, Hum. Mol. Genet. 11 (16) (2002) 1865–1877.
[23] M.V. Busi, E.J. Zabaleta, A. Araya, D.F. Gomez-Casati, Functional and molecular characterization of the frataxin homolog from Arabidopsis thaliana, FEBS Lett. 576 (1–2) (2004) 141–144.
[24] V. Vazzola, A. Losa, C. Soave, I. Murgia, Knockout of frataxin gene causes embryo lethality in Arabidopsis, FEBS Lett. 581 (4) (2007) 667–672.
[25] M. Martin, M.J. Colman, D.F. Gomez-Casati, L. Lamattina, E.J. Zabaleta, Nitric oxide accumulation is required to protect against iron-mediated oxidative stress in frataxin-deficient Arabidopsis plants, FEBS Lett. 583 (3) (2009) 542–548.
[26] J. Priller, C.R. Scherzer, P.W. Faber, M.E. MacDonald, A.B. Young, Frataxin gene of Friedreich's ataxia is targeted to mitochondria, Ann. Neurol. 42 (2) (1997) 265–269.
[27] P. Cavadini, J. Adamec, F. Taroni, O. Gakh, G. Isaya, Two-step processing of human frataxin by mitochondrial processing peptidase. Precursor and intermediate forms are cleaved at different rates, J. Biol. Chem. 275 (52) (2000) 41469–41475.
[28] D.M. Gordon, Q. Shi, A. Dancis, D. Pain, Maturation of frataxin within mammalian and yeast mitochondria: one-step processing by matrix processing peptidase, Hum. Mol. Genet. 8 (12) (1999) 2255–2262.
[29] S.S. Branda, P. Cavadini, J. Adamec, F. Kalousek, F. Taroni, G. Isaya, Yeast and human frataxin are processed to mature form in two sequential steps by the mitochondrial processing peptidase, J. Biol. Chem. 274 (32) (1999) 22763–22769.
[30] H. Koutnikova, V. Campuzano, M. Koenig, Maturation of wild-type and mutated frataxin by the mitochondrial processing peptidase, Hum. Mol. Genet. 7 (9) (1998) 1485–1489.
[31] V.R. Turowski, C. Aknin, M.V. Maliandi, C. Buchensky, L. Leaden, D.A. Peralta, M.V. Busi, A. Araya, D.F. Gomez-Casati, Frataxin is localized to both the chloroplast and mitochondrion and is involved in chloroplast Fe-S protein function in Arabidopsis, PLoS One 10 (10) (2015) e0141443.
[32] I. Murgia, D. Tarantino, C. Soave, Mitochondrial iron metabolism in plants: frataxin comes into play, Plant Soil 325 (1) (2009) 5–14.
[33] I. Small, N. Peeters, F. Legeai, C. Lurin, Predotar: a tool for rapidly screening proteomes for N-terminal targeting sequences, Proteomics 4 (6) (2004) 1581–1590.
[34] O. Emanuelsson, H. Nielsen, S. Brunak, G. von Heijne, Predicting subcellular localization of proteins based on their N-terminal amino acid sequence, J. Mol. Biol. 300 (4) (2000) 1005–1016.
[35] M.A. Larkin, G. Blackshields, N.P. Brown, R. Chenna, P.A. McGettigan, H. McWilliam, F. Valentin, I.M. Wallace, A. Wilm, R. Lopez, J.D. Thompson,

T.J. Gibson, D.G. Higgins, W. Clustal, X. Clustal, Version 2.0, Bioinformatics 23 (21) (2007) 2947–2948.
[36] K. Tamura, D. Peterson, N. Peterson, G. Stecher, M. Nei, S. Kumar, MEGA5: molecular evolutionary genetics analysis using maximum likelihood, evolutionary distance, and maximum parsimony methods, Mol. Biol. Evol. 28 (10) (2011) 2731–2739.
[37] J.L. Pons, G. Labesse, @TOME-2: a new pipeline for comparative modeling of protein-ligand complexes, Nucleic Acids Res. 37 (Web Server issue) (2009) W485–W491.
[38] M.J. Sippl, Recognition of errors in three-dimensional structures of proteins, Proteins 17 (4) (1993) 355–362.
[39] M. Wiederstein, M.J. Sippl, ProSA-web: interactive web service for the recognition of errors in three-dimensional structures of proteins, Nucleic Acids Res. 35 (Web Server issue) (2007) W407–W410.
[40] R. Luthy, J.U. Bowie, D. Eisenberg, Assessment of protein models with three-dimensional profiles, Nature 356 (6364) (1992) 83–85.
[41] R. Maiti, G.H. Van Domselaar, H. Zhang, D.S. Wishart, SuperPose: a simple server for sophisticated structural superposition, Nucleic Acids Res. 32 (Web Server issue) (2004) W590–W594.
[42] M.G. Claros, P. Vincens, Computational method to predict mitochondrially imported proteins and their targeting sequences, Eur. J. Biochem. 241 (3) (1996) 779–786.
[43] O. Emanuelsson, H. Nielsen, G. von Heijne, ChloroP, a neural network-based method for predicting chloroplast transit peptides and their cleavage sites, Protein Sci. 8 (5) (1999) 978–984.
[44] S.J. Clough, A.F. Bent, Floral dip: a simplified method for Agrobacterium-mediated transformation of Arabidopsis thaliana, Plant J. 16 (6) (1998) 735–743.
[45] S.D. Yoo, Y.H. Cho, J. Sheen, Arabidopsis mesophyll protoplasts: a versatile cell system for transient gene expression analysis, Nat. Protoc. 2 (7) (2007) 1565–1572.
[46] U.K. Laemmli, Cleavage of structural proteins during the assembly of the head of bacteriophage T4, Nature 227 (5259) (1970) 680–685.
[47] M.M. Bradford, A rapid and sensitive method for the quantitation of microgram quantities of protein utilizing the principle of protein-dye binding, Anal. Biochem. (1976) 248–254.
[48] S.W. Provencher, J. Glockner, Estimation of globular protein secondary structure from circular dichroism, Biochemistry 20 (1) (1981) 33–37.
[49] N. Sreerama, R.W. Woody, Estimation of protein secondary structure from circular dichroism spectra: comparison of CONTIN, SELCON, and CDSSTR methods with an expanded reference set, Anal. Biochem. 287 (2) (2000) 252–260.
[50] S. Dhe-Paganon, R. Shigeta, Y.I. Chi, M. Ristow, S.E. Shoelson, Crystal structure of human frataxin, J. Biol. Chem. 275 (40) (2000) 30753–30756.
[51] S.J. Cho, M.G. Lee, J.K. Yang, J.Y. Lee, H.K. Song, S.W. Suh, Crystal structure of Escherichia coli CyaY protein reveals a previously unidentified fold for the evolutionarily conserved frataxin family, Proc. Natl. Acad. Sci. U. S. A 97 (16) (2000) 8932–8937.
[52] S.E. Faraj, E.A. Roman, M. Aran, M. Gallo, J. Santos, The alteration of the C-terminal region of human frataxin distorts its structural dynamics and function, FEBS J. 281 (15) (2014) 3397–3419.
[53] C. Carrie, E. Giraud, J. Whelan, Protein transport in organelles: dual targeting of proteins to mitochondria and chloroplasts, FEBS J. 276 (5) (2009) 1187–1195.
[54] N. Peeters, I. Small, Dual targeting to mitochondria and chloroplasts, Biochim. Biophys. Acta 1541 (1–2) (2001) 54–63.
[55] S.M. Marino, V.N. Gladyshev, Cysteine function governs its conservation and degeneration and restricts its utilization on protein surfaces, J. Mol. Biol. 404 (5) (2010) 902–916.
[56] R.S. Wible, T.R. Sutter, Soft Cysteine Signaling Network: the functional significance of cysteine in protein function and the soft acid/base thiol chemistry that facilitates cysteine modification, Chem. Res. Toxicol. (2017).
[57] M. Zheng, F. Aslund, G. Storz, Activation of the OxyR transcription factor by reversible disulfide bond formation, Science 279 (5357) (1998) 1718–1721.
[58] D. Azevedo, F. Tacnet, A. Delaunay, C. Rodrigues-Pousada, M.B. Toledano, Two redox centers within Yap1 for H2O2 and thiol-reactive chemicals signaling, Free Radic. Biol. Med. 35 (8) (2003) 889–900.
[59] J.T. Vivian, P.R. Callis, Mechanisms of tryptophan fluorescence shifts in proteins, Biophys. J. 80 (5) (2001) 2093–2109.
[60] S. Leidgens, S. De Smet, F. Foury, Frataxin interacts with Isu1 through a conserved tryptophan in its beta-sheet, Hum. Mol. Genet. 19 (2) (2010) 276–286.
[61] B. Ma, T. Elkayam, H. Wolfson, R. Nussinov, Protein-protein interactions: structurally conserved residues distinguish between binding sites and exposed protein surfaces, Proc. Natl. Acad. Sci. U. S. A 100 (10) (2003) 5772–5777.
[62] P. Gonzalez-Cabo, F. Palau, Mitochondrial pathophysiology in Friedreich's ataxia, J. Neurochem. 126 (Suppl 1) (2013) 53–64.
[63] J. Balk, S. Lobreaux, Biogenesis of iron-sulfur proteins in plants, Trends Plant Sci. 10 (7) (2005) 324–331.
[64] J. Balk, M. Pilon, Ancient and essential: the assembly of iron-sulfur clusters in plants, Trends Plant Sci. 16 (4) (2011) 218–226.
[65] J. Adamec, F. Rusnak, W.G. Owen, S. Naylor, L.M. Benson, A.M. Gacy, G. Isaya, Iron-dependent self-assembly of recombinant yeast frataxin: implications for Friedreich ataxia, Am. J. Hum. Genet. 67 (3) (2000) 549–562.
[66] P. Cavadini, H.A. O'Neill, O. Benada, G. Isaya, Assembly and iron-binding properties of human frataxin, the protein deficient in Friedreich ataxia, Hum. Mol. Genet. 11 (3) (2002) 217–227.